

Interaction range and temperature dependence of symmetry breaking in strongly correlated 2D moiré TMD bilayers

Haining Pan¹ and Sankar Das Sarma¹

¹*Condensed Matter Theory Center and Joint Quantum Institute, Department of Physics, University of Maryland, College Park, Maryland 20742, USA*

We theoretically consider 2D transition metal dichalcogenide (TMD) moiré bilayers, which are strongly correlated in the sense that the on-site Coulomb interaction is comparable to or larger than the hopping kinetic energy between the moiré lattice sites. The system accommodates many symmetry-broken ground states both in charge and isospin sectors at various commensurate rational fillings such as 1/2, 1/3, 1/4, 2/3, etc. We investigate two complementary important aspects of the dependence of the symmetry breaking on: (1) the range of the electron-electron interaction, which can in principle be experimentally controlled by the nearby gates and the dielectric environment; (2) temperature, which could thermally suppress the symmetry breaking above a critical temperature. Experimental implications of the theory are discussed.

Introduction.— Moiré 2D TMD bilayers have recently emerged as a tunable interacting lattice system to study strong correlation effects in semiconductor layers [1–14]. It was pointed out that these systems are ideal analog solid state emulators of the 2D Hubbard model in the strongly correlated regime with $U/t \sim O(1)$, where U, t are the usual effective electron interaction and noninteracting kinetic energy scales, respectively, as appearing in the Hubbard model [15–22]. Various charge and isospin symmetry broken phases have been theoretically predicted and experimentally observed in both TMD homo- and hetero-bilayers (sometimes in the presence of an applied perpendicular electric field V_z , which modifies the noninteracting band structure, further enhancing the dimensionless interaction strength), and there is general agreement between theory and experiment although theory seems to predict richer exotic possibilities (e.g., spin liquids, superconductors) than have been experimentally validated so far. But the most significant theoretical predictions of correlated insulators at half-filling and the existence of generalized Wigner crystal type charge density waves (CDW) have been directly verified experimentally [8]. Also, the predicted doping- and field-tuned insulator to metal transitions have also been recently observed [9, 13, 21] at half-filling, but the role of disorder is likely to be important in such transitions [23]. The subject is undoubtedly among the most active topics in all of condensed matter and strong correlation physics, and as such, many important questions remain unaddressed.

In the current work, we investigate two such open questions, finding some surprising results. The paper consists of two complementary issues, both with immediate and important experimental and theoretical significance. The first topic is the role of the interaction range on the symmetry breaking phenomenon. In particular, the bare inter-particle (electron or hole) interaction is by definition the long-ranged Coulomb interaction screened by the environment, and thus a minimal Hubbard model with just moiré on-site interaction with a single U is inappropriate for TMDs. We systematically investigate the effect of longer range coupling between far away moiré sites on

the ground state symmetry breaking, finding that symmetry breaking may actually sometimes be suppressed by having distant neighbor Coulomb coupling, a result which sounds counterintuitive, but is nevertheless correct. The second topic we study is the thermal suppression of the symmetry broken phase with the charge gap vanishing at a critical temperature, as has recently been reported experimentally [13].

Theory.—Our model is a generalized Hubbard model on a triangular moiré lattice realized in a twisted homobilayer WSe₂ as per

$$H = \sum_s \sum_{i,j} t_s (\mathbf{R}_i - \mathbf{R}_j) c_{i,s}^\dagger c_{j,s} + \frac{1}{2} \sum_{s,s'} \sum_{i,j} U(\mathbf{R}_i - \mathbf{R}_j) c_{i,s}^\dagger c_{j,s'}^\dagger c_{j,s'} c_{i,s}, \quad (1)$$

where $t_s (\mathbf{R}_i - \mathbf{R}_j)$ is the hopping between the moiré lattice site i and j , fitted from the first moiré valence band of twisted WSe₂ at $\pm K$ valleys in the noninteracting picture, and $s = \uparrow$ and \downarrow are coupled with the $+K$ and $-K$ valleys [19]. $U(\mathbf{R}_i - \mathbf{R}_j)$ describes the Coulomb repulsion between site i and j . We control the range of the Coulomb interactions by including a finite number of neighbors coupled in the theory. These neighbors are denoted by hexagonal “shells” (e.g., onsite interaction U_0 is 0-shell, 1-shell means six nearest-neighbor interactions U_1 plus U_0) in the following results. By comparing the results of short-range (few shells) and long-range (many shells) interactions, we investigate the role of the interaction range.

To find the ground states of Eq. (1), which contains quartic terms, at the mean-field level, we use the Hartree-Fock approximation to expand the quartic interaction (the second term in Eq. (1)) into quadratic terms as $\sum_{s,s'} \sum_{i,j} U(\mathbf{R}_i - \mathbf{R}_j) (\langle c_{i,s}^\dagger c_{i,s} \rangle c_{j,s'}^\dagger c_{j,s'} - \langle c_{i,s}^\dagger c_{j,s'} \rangle c_{j,s'}^\dagger c_{i,s})$, and diagonalize the quadratic Hamiltonian in the momentum space to find the self-consistent solution starting from a given initial ansatz. In the end, we obtain the

energetically-favorable ground state by comparing the energies of various candidate phases (Mott insulator, correlated insulator, normal metal, etc). We refer the reader for the details to Ref. 20.

To address the second question, we consider the finite-temperature thermal state at a fixed filling factor. Here, the temperature enters through the correlator $\langle c_{i,s}^\dagger c_{j,s'} \rangle$, which is averaged with respect to the occupation number of each state with energy E , where the occupation number follows the Fermi-Dirac distribution $f_T(E) = \{1 + \exp[(E - \mu)/T]\}^{-1}$ at temperature T . At finite temperature, we define the filling factor by the average number of holes per site as $\nu = \frac{1}{N} \sum_{i,s} \langle c_{i,s}^\dagger c_{i,s} \rangle$, where N is the total number of moiré sites in the system, and $\nu = 0$ corresponds to the charge neutrality point. Thus, the chemical potential μ must be adjusted in each iteration to ensure the invariance of the filling factor ν . To study the metal-insulator transition (MIT) driven by temperature T , we use the charge gap E_G , defined by the extra energy of adding one hole to the system, as the order parameter of the insulating phase ($E_G > 0$) and metallic phase ($E_G = 0$), following the experiment [13].

The phase transitions in moiré TMD are extremely rich as they can be driven by many different parameters, such as the interaction range, V_z , ϵ , θ , ν , and T . Here, the interaction range determines the nature of the interaction in Eq. (1): whether it is a short-range screened Coulomb interaction or a long-range pure Coulomb interaction. The perpendicular electric field V_z effectively generates a Dzyaloshinskii-Moriya interaction at $\nu = 1$ [19], which alters the single-particle band structure, and, consequently, changes the magnitude adding a complex phase to the hopping parameter t in Eq. (1) (refer to Fig. 10 in Ref. 19 for the magnitude and phase of t as a function of V_z). The dielectric constant ϵ and the twist angle θ control the strength of Coulomb interaction and hopping, respectively, which can induce the transition from ferromagnetic to antiferromagnetic order by changing the exchange energy t^2/U . The temperature T can thermally suppress the insulating energy gap to induce a MIT.

Results and Discussion.—We first set the electric field V_z and temperature T to zero to investigate the interaction range. Here, the short-range interaction means only onsite (for $\nu = 1$) or onsite plus nearest-neighbor (for $\nu < 1$). The long-range interaction means distant neighbors (up to 200-shell) are coupled by U in the theory. We use the strict Coulomb interaction, $V(r) = e^2/(\epsilon r)$, where r is the Wannier-weighted inter-particle separation as appropriate for the TMD moiré system and ϵ is the effective background dielectric constant including the substrates, and calculate the mean-field Hartree-Fock quantum phase diagram numerically self-consistently starting from the classical ansatz for the charge density wave states as in Refs. 19 and 20. We show in Fig. 1 the resultant $\epsilon - \theta$ phase diagrams for filling $\nu = 1, 1/3, 2/3$ where $\nu = 1$ implies one hole per moiré unit cell (i.e., half-filled in the usual Mott-Hubbard terminology). For each fill-

ing, we show side by side the results for just short range (left panels) and long range (right panels), where the results have basically converged to the infinite shell limit. The results presented in Fig. 1 involve many hours of high-performance computing, as we must first carry out the moiré band structure calculation for each value of ϵ and θ , and then do the time-intensive many-body self-consistent calculations to obtain the full phase diagram. We refer the reader to Refs. 19 and 20 on the details of these phases.

The results in Fig. 1 are surprising to say the least: For example, in Figs. 1(a-b) at $\nu = 1$, the system undergoes a MIT from an insulator with 120° antiferromagnetic Neél state [denoted by “AFM-No-I($\sqrt{3} \times \sqrt{3}$)” in Fig. 1(g)] to normal gapless metallic phase as θ increases or ϵ increases. The normal gapless metallic phase (i.e., the non-symmetry-broken phase corresponding to the noninteracting band structure prediction at half-filling) is preferred for large ϵ and θ by the full long-range interaction [Fig. 1(b)] over the corresponding 0-shell short-range interaction calculation [Fig. 1(a)] although the 200-shell calculation includes U_0 and U_1 and a large number of additional interaction terms all the way to 200-shell! A similar situation also arises for $\nu = 1/3$ (i.e., 1/6 filling) in Figs. 1(c-d), where the full long-range 200-shell calculation [Fig. 1(d)] has a much larger regime of the non-symmetry-broken normal gapless metallic phase than the calculation including only U_0 and U_1 [Fig. 1(c)]. By contrast, the $\nu = 2/3$ (i.e., 1/3 filling) manifests more complicated behavior for the full 200-shell long-range theory [Fig. 1(f)] than the short-range $U_0 + U_1$ model [Fig. 1(e)], with the normal metallic phase (upper right hand corner) being a symmetry-broken ferromagnetic metallic phase rather than a normal nonmagnetic metal as for the $U_0 + U_1$ short-range model. In addition, the dominant state “AFM-HC-I($\sqrt{3} \times \sqrt{3}$)” [Fig. 1(l)] with antiferromagnetic order switches to “FM-HC-I($\sqrt{3} \times \sqrt{3}$)” [Fig. 1(k)] with ferromagnetic order. The qualitative difference between the predicted phase diagrams in the short-range and long-range interaction models can be understood as arising from a subtle interplay between hopping, Pauli principle, and interaction range, which has no generic easy and intuitive explanation. It is easy to see in a 1D lattice that having just the on-site interaction and simply adding one next-nearest-neighbor interaction term drastically alters the configuration-dependent local ground state energetics, and the situation is obviously extremely complex on a 2D triangular lattice with multiple hopping and interaction terms with no easy and obvious explanations for the details of the phase diagram—one must do the calculation to obtain the correct ground states, and as is obvious from Fig. 1, making the standard on-site Hubbard model approximation uncritically may be misleading.

Our results in Fig. 1 are just not surprising, they have clear experimental implications since, in principle, the interaction range can be controlled by introducing metallic gates close to the TMD bilayer. In addition, samples with

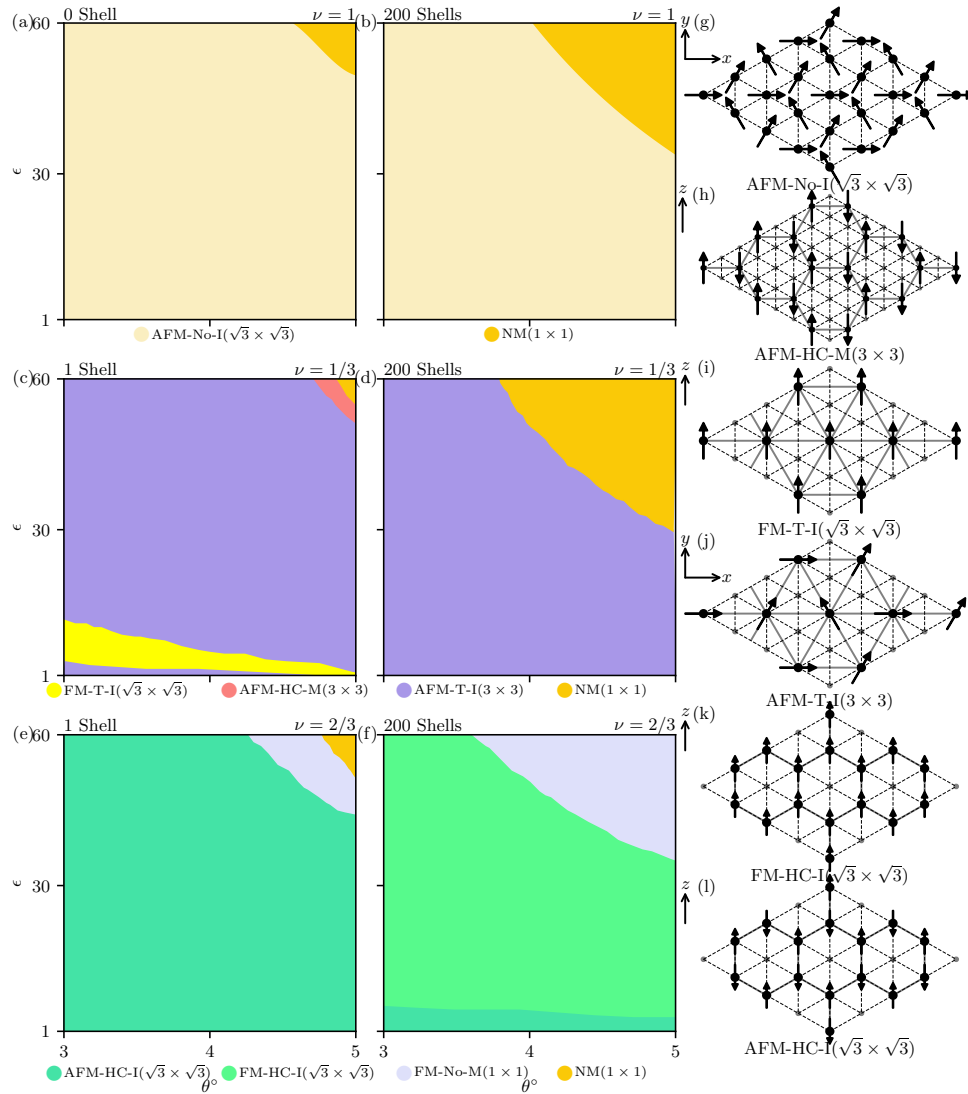


FIG. 1. Phase diagrams as a function of the twist angle θ and dielectric constant ϵ at (a-b) $\nu = 1$; (c-d) $\nu = 1/3$; (e-f) $\nu = 2/3$. The left column is for the short-range interaction while the right column is for the long-range interaction. Here ‘T’ means the triangular lattice, ‘HC’ means the honeycomb lattice, ‘No’ means no CDW, ‘NM’ means spinless normal metal, ‘M’ means the phase is a metal, and ‘I’ means the phase is an insulator. The numbers in the bracket indicate the extended periods of each phase which are shown in (g-l).

varying θ and varying background dielectric constant (by using different substrates) can be fabricated to directly verify that the resultant quantum phase diagram depends quite sensitively on the interaction range. It is actually possible that our predictions of Fig. 1 have already been verified experimentally as samples from different laboratories do not always reflect the same symmetry broken phases, but without a systematic experimental study, one cannot be sure that the striking physics predicted in Fig. 1 has been observed.

In discussing the thermal MIT and a possible critical temperature at $\nu=1$, as observed recently [13], we focus on $\nu=1$ and consider only the 0-shell theory, which agrees with the full long-range results up to large ϵ (< 30) according to Figs. 1(a-b). It is important to realize that

the charge gap can be closed even at $T=0$ causing a MIT by tuning ϵ (controlling interaction), θ (controlling hopping), or an applied electric field V_z which also modifies the single-particle band structure affecting the effective correlation parameter U/t . In Fig. 2(a), we first provide our calculated phase diagram as a function of θ and V_z at $T=0$ using the same self-consistent mean-field Hartree-Fock theory as used for Fig. 1 [19]. We fix $\epsilon = 20$ for these calculations, which is our best estimate for the screening environment for Ref. 13 including both the substrate and the gate-induced screening. (Results for other ϵ values are similar with the gap energies and phase boundary being quantitatively different.) The phase boundary of the metal-insulator transition is indicated by the red dashed line, where the metallic phase prefers large twist angles θ

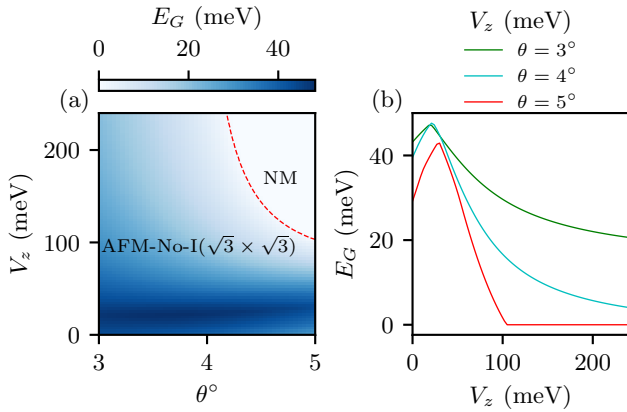


FIG. 2. (a) Charge gap E_G as a function of the twist angle θ and the electric field V_z at $\epsilon = 20$ and $\nu = 1$. The red dashed line is the phase boundary between “AFM-No-I($\sqrt{3} \times \sqrt{3}$)” and normal metal. (b) Linecuts of the charge gap E_G as a function of V_z for $\theta = 3^\circ$ (green), $\theta = 4^\circ$ (blue), and $\theta = 5^\circ$ (red).

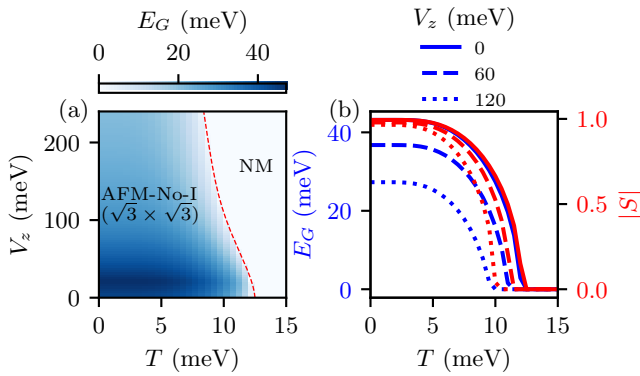


FIG. 3. (a) Charge gap as a function of the electric field V_z and the temperature T at $\theta = 3^\circ$, $\nu = 1$ and $\epsilon = 20$. The red dashed line indicates the T_c , which is the phase boundary between “AFM-No-I($\sqrt{3} \times \sqrt{3}$)” and normal metal. (b) Linecuts of the charge gap E_G (blue, left axis) and the spin magnitude $|S|$ (red, right axis) as a function of the temperature T for $V_z = 0$ (solid line), $V_z = 60$ meV (dashed line), and $V_z = 120$ meV (dotted line).

and large V_z . We see from Fig. 2(b) that large V_z by itself can close the charge gap of the antiferromagnetic insulating phase at $V_z \sim 100$ meV for $\theta = 5^\circ$ (red line), but not for a smaller twist angle [e.g., $\theta = 3^\circ$ (green line)]. So, our first prediction, consistent with recent experiments, is that finite V_z would cause an insulator-to-metal Mott transition at half-filling for larger twist angles.

Since the metal-insulator transition cannot be induced by V_z for the small angle ($\theta \sim 3^\circ$), an interesting question is whether the finite temperature can induce a MIT by thermally suppressing the charge gap. In Fig. 3, we show our calculated mean-field thermal $T - V_z$ phase diagram for $\nu=1$, $\theta = 3^\circ$, and $\epsilon=20$. We emphasize that V_z by itself cannot cause a MIT at $\theta = 3^\circ$, with the ground state being the “AFM-No-I($\sqrt{3} \times \sqrt{3}$)” with a charge gap for all V_z , but finite temperature destroys the symmetry-broken long-range order through thermal fluctuations with a critical $T_c \sim 10$ meV (which is an upper bound since our mean-field treatment ignores fluctuations). We note two experimentally-verifiable important features of Fig. 3: (1) T_c [the red dashed line in Fig. 3(a)] does not depend strongly on V_z , with T_c varying by less than 25% for very large changes (from 0 to 240 meV) in V_z ; (2) both the charge gap E_G [blue lines in Fig. 3(b)] and the spin texture, denoted by its magnitude $|S|$ [red lines in Fig. 3(b)], drop to zero at the same T_c for all V_z (solid, dashed, and dotted lines corresponding to the results at $V_z=0$, 60, and 120 meV respectively). The suppression of the charge gap E_G and spin magnitude $|S|$ as a function of temperature manifests a typical feature of self-consistent solutions from the mean-field Hamiltonian. The phase for $T > T_c$ is thus a gapless paramagnetic normal metal with no long range spin ordering. This is also a verifiable prediction. The fact that the thermal suppression of the antiferromagnetic insulator phase (“AFM-No-I($\sqrt{3} \times \sqrt{3}$)” is not sensitively dependent on V_z [rather obvious in Fig. 3(a)] is another verifiable prediction.

Conclusion.— We study theoretically the quantum phase diagrams of moiré TMD systems, addressing the complementary physics of the effects of interaction range, applied electric field, and temperature on the symmetry breaking properties. We find that increasing interaction range has an apparent surprising effect of actually suppressing the symmetry breaking in some situations. We calculate the finite-temperature TMD thermal phase diagram, finding that both the charge gap and the spin texture disappear at half-filling above a critical temperature simultaneously, leading to a thermal phase transition from an antiferromagnetic gapped insulator to a gapless paramagnetic metal. Our predictions are directly experimentally verifiable, and both the temperature-induced and the electric field-induced insulator-to-metal transition at half-filling have already been observed [9, 13].

This work is supported by the Laboratory for Physical Sciences. We also acknowledge the support of the University of Maryland High-Performance Computing Cluster (HPCC).

[1] E. C. Regan, D. Wang, C. Jin, M. I. Bakti Utama, B. Gao, X. Wei, S. Zhao, W. Zhao, Z. Zhang, K. Yumigeta, M. Blei, J. D. Carlström, K. Watanabe, T. Taniguchi, S. Tongay, M. Crommie, A. Zettl, and

F. Wang, Mott and generalized Wigner crystal states in WSe₂/WS₂ moiré superlattices, *Nature* **579**, 359 (2020).
[2] L. Wang, E.-M. Shih, A. Ghiotto, L. Xian, D. A. Rhodes, C. Tan, M. Claassen, D. M. Kennes, Y. Bai, B. Kim,

K. Watanabe, T. Taniguchi, X. Zhu, J. Hone, A. Rubio, A. N. Pasupathy, and C. R. Dean, Correlated electronic phases in twisted bilayer transition metal dichalcogenides, *Nature Materials* **19**, 861 (2020).

[3] Y. Xu, S. Liu, D. A. Rhodes, K. Watanabe, T. Taniguchi, J. Hone, V. Elser, K. F. Mak, and J. Shan, Correlated insulating states at fractional fillings of moiré superlattices, *Nature* **587**, 214 (2020).

[4] Z. Zhang, Y. Wang, K. Watanabe, T. Taniguchi, K. Ueno, E. Tutuc, and B. J. LeRoy, Flat bands in twisted bilayer transition metal dichalcogenides, *Nature Physics* **16**, 1093 (2020).

[5] Y. Zhou, J. Sung, E. Brutschea, I. Esterlis, Y. Wang, G. Scuri, R. J. Gelly, H. Heo, T. Taniguchi, K. Watanabe, G. Zaránd, M. D. Lukin, P. Kim, E. Demler, and H. Park, Bilayer Wigner crystals in a transition metal dichalcogenide heterostructure, *Nature* **595**, 48 (2021).

[6] Y. Tang, L. Li, T. Li, Y. Xu, S. Liu, K. Barmak, K. Watanabe, T. Taniguchi, A. H. MacDonald, J. Shan, and K. F. Mak, Simulation of Hubbard model physics in WSe₂/WS₂ moiré superlattices, *Nature* **579**, 353 (2020).

[7] E. Liu, T. Taniguchi, K. Watanabe, N. M. Gabor, Y.-T. Cui, and C. H. Lui, Excitonic and Valley-Polarization Signatures of Fractional Correlated Electronic Phases in a WSe₂/WS₂ Moiré Superlattice, *Phys. Rev. Lett.* **127**, 037402 (2021).

[8] H. Li, S. Li, E. C. Regan, D. Wang, W. Zhao, S. Kahn, K. Yumigeta, M. Blei, T. Taniguchi, K. Watanabe, S. Tongay, A. Zettl, M. F. Crommie, and F. Wang, Imaging two-dimensional generalized Wigner crystals, *Nature* **597**, 650 (2021).

[9] T. Li, S. Jiang, L. Li, Y. Zhang, K. Kang, J. Zhu, K. Watanabe, T. Taniguchi, D. Chowdhury, L. Fu, J. Shan, and K. F. Mak, Continuous Mott transition in semiconductor moiré superlattices, *Nature* **597**, 350 (2021).

[10] T. Li, S. Jiang, B. Shen, Y. Zhang, L. Li, T. Devakul, K. Watanabe, T. Taniguchi, L. Fu, J. Shan, and K. F. Mak, Quantum anomalous Hall effect from intertwined moiré bands, [arXiv:2107.01796](https://arxiv.org/abs/2107.01796) (2021).

[11] X. Huang, T. Wang, S. Miao, C. Wang, Z. Li, Z. Lian, T. Taniguchi, K. Watanabe, S. Okamoto, D. Xiao, S.-F. Shi, and Y.-T. Cui, Correlated insulating states at fractional fillings of the WS₂/WSe₂ moiré lattice, *Nature Physics* **17**, 715 (2021).

[12] C. Jin, Z. Tao, T. Li, Y. Xu, Y. Tang, J. Zhu, S. Liu, K. Watanabe, T. Taniguchi, J. C. Hone, L. Fu, J. Shan, and K. F. Mak, Stripe phases in WSe₂/WS₂ moiré superlattices, *Nature Materials* **20**, 940 (2021).

[13] A. Ghiotto, E.-M. Shih, G. S. S. G. Pereira, D. A. Rhodes, B. Kim, J. Zang, A. J. Millis, K. Watanabe, T. Taniguchi, J. C. Hone, L. Wang, C. R. Dean, and A. N. Pasupathy, Quantum criticality in twisted transition metal dichalcogenides, *Nature* **597**, 345 (2021).

[14] T. Li, J. Zhu, Y. Tang, K. Watanabe, T. Taniguchi, V. Elser, J. Shan, and K. F. Mak, Charge-order-enhanced capacitance in semiconductor moiré superlattices, *Nat. Nanotechnol.* **16**, 1068 (2021).

[15] F. Wu, T. Lovorn, E. Tutuc, and A. H. MacDonald, Hubbard model physics in transition metal dichalcogenide moiré bands, *Phys. Rev. Lett.* **121**, 026402 (2018).

[16] N. C. Hu and A. H. MacDonald, Competing magnetic states in transition metal dichalcogenide moiré materials, [arXiv:2108.02159](https://arxiv.org/abs/2108.02159) (2021).

[17] N. Morales-Durán, N. C. Hu, P. Potasz, and A. H. MacDonald, Non-local interactions in moiré Hubbard systems, [arXiv:2108.03313](https://arxiv.org/abs/2108.03313) (2021).

[18] N. Morales-Durán, A. H. MacDonald, and P. Potasz, Metal-insulator transition in transition metal dichalcogenide heterobilayer moiré superlattices, *Phys. Rev. B* **103**, L241110 (2021).

[19] H. Pan, F. Wu, and S. Das Sarma, Band topology, Hubbard model, Heisenberg model, and Dzyaloshinskii-Moriya interaction in twisted bilayer WSe₂, *Phys. Rev. Research* **2**, 033087 (2020).

[20] H. Pan, F. Wu, and S. Das Sarma, Quantum phase diagram of a Moiré-Hubbard model, *Phys. Rev. B* **102**, 201104 (2020).

[21] H. Pan and S. Das Sarma, Interaction-Driven Filling-Induced Metal-Insulator Transitions in 2D Moiré Lattices, *Phys. Rev. Lett.* **127**, 096802 (2021).

[22] J. Zang, J. Wang, J. Cano, and A. J. Millis, Hartree-Fock study of the moiré Hubbard model for twisted bilayer transition metal dichalcogenides, *Phys. Rev. B* **104**, 075150 (2021).

[23] S. Ahn and S. D. Sarma, Disorder induced 2D metal-insulator transition in moiré transition metal dichalcogenide multilayers, [arXiv:2108.07271](https://arxiv.org/abs/2108.07271) (2021).